SWIFT-XRT-CALDB-04

Release Date: Jul 10th, 2018

Prepared by: Andrew Beardmore, Kim Page, Claudio Pagani (UL), Matteo Perri, Milvia Capalbi (ASDC)

Date revised: July 1st, 2018

Revision: 18

Revised by: Andrew Beardmore & Claudio Pagani

SWIFT-XRT CALDB RELEASE NOTE

SWIFT-XRT-CALDB-04: Gain

1 Component Files

Table 1: Latest CALDB component files.

FILENAME	VALID DATE	RELEASE DATE	REVISION
swxpcgains6_20010101v017.fits[a]	01-Jan-2001	10-Jul-2018	18
swxwtgains6_20010101v019.fits[a]	01-Jan-2001	10-Jul-2018	18

[a] 's6' refers to $V_{ss} = 6$ V gain files. The substrate voltage was raised permanently to this value on 2007-Aug-30 at 14:25UT.

2 Introduction

This document contains a description of the analysis performed at Leicester University to produce the gain calibration products for the *Swift*-XRT Calibration Database (CALDB).

Section 3.1 describes the updates to the gain files in this release and illustrates their quality and limitations. Section 4 summarizes changes to *Swift* operations during the mission that had a significant impact on the gain characterisation, such as the substrate voltage change, the charge traps analysis and corrections, and the modifications to the gain files and software to account for these changes. Appendix A illustrates the derivation of the gain and CTI coefficients and their implementation in the CALDB gain files. Appendix B describes the gain and CTI measurements, while the charge traps analysis is shown in Appendix C. Appendix E lists the previous gain file releases.

3 Updates to the Gain Files

3.1 New Release (Revision 18) Summary

Radiation damage causes degradation to the CCD spectral response due to the build up of charge trapping sites in the Si crystalline structure, which retain charge, resulting in incomplete X-ray event energy reconstruction. Updates to the gain and CTI coefficients (Section 3.3), as well as the charge trap corrections table (Section 3.4), help maintain the accuracy of the gain corrected energy scale and partially recover the spectral resolution (see tables 2 and 3).

Observations of the Tycho and Cas A supernova remnants are scheduled once a year to monitor the evolution of the spectral response of the CCD, using their strong Si-Kα lines. The observing strategy employed to acquire the trap calibration data was the same as that used for the previous release (see release note SWIFT-XRT-CALDB-04_v17) and is summarised in Figure 1. For Photon Counting (PC) mode, 15×20ks pointings of the Tycho SNR were obtained from August – December 2017, spread over the entire CCD, but with the greatest exposure covering the central 200×400 pixels (where the majority of XRT observations are performed). For Windowed Timing (WT) mode, 6×10ks pointings of Cas A were taken from December 2017 – January 2018, covering the central 200×300 pixels.

When the PC mode Tycho observations are processed with the previous version of the PC gain file (i.e. v016, swxpcgains6_20010101v016.fits), energy shifts of the silicon [iron] emission lines of ~ 30 [110] eV are seen with respect to the expected reference values when averaged over the entire CCD. Similarly, when the WT mode Cas A data are processed with the previous version of the WT gain file (v018, swxwtgains6_20010101v018.fits), energy shifts of the silicon [iron] emission lines of ~ 50 [130] eV are seen over the central 200 rows of the CCD.

To restore the accuracy of the gain corrected energy scale, incrementally updated versions of the PC (**swxpcgains6_20010101v017.fits**) and WT (**swxwtgains6_20010101v019.fits**) gain files have been generated and are included in this release. The updates include:

- New gain and CTI coefficients, derived from the analysis of the corner source data collected from November 2016 to May 2018;
- Updated PC charge trap correction tables for existing traps, measured using the Si-Kα line from the Tycho calibration observations taken in August-December 2017 and applied from August 2017;
- New WT charge trap correction tables created from measurements of the Si-Kα line from the Cas A calibration observations taken in December 2017 – January 2018, applied from September 2017;
- Updated modelling of the energy dependence of the PC mode trap corrections (based on new observations of SNR E0102 and the soft NS RX J1856.5-3754 at low energies ($\lesssim 1$ keV) and Tycho at higher energies ($\gtrsim 1$ keV));
- Updated modelling of the energy dependence of the WT mode trap corrections (based on new observations of the SNRs E0102, N132D and the soft NS RX J1856.5-3754 at low energies ($\lesssim 1$ keV) and Cas A at higher energies ($\gtrsim 1$ keV));

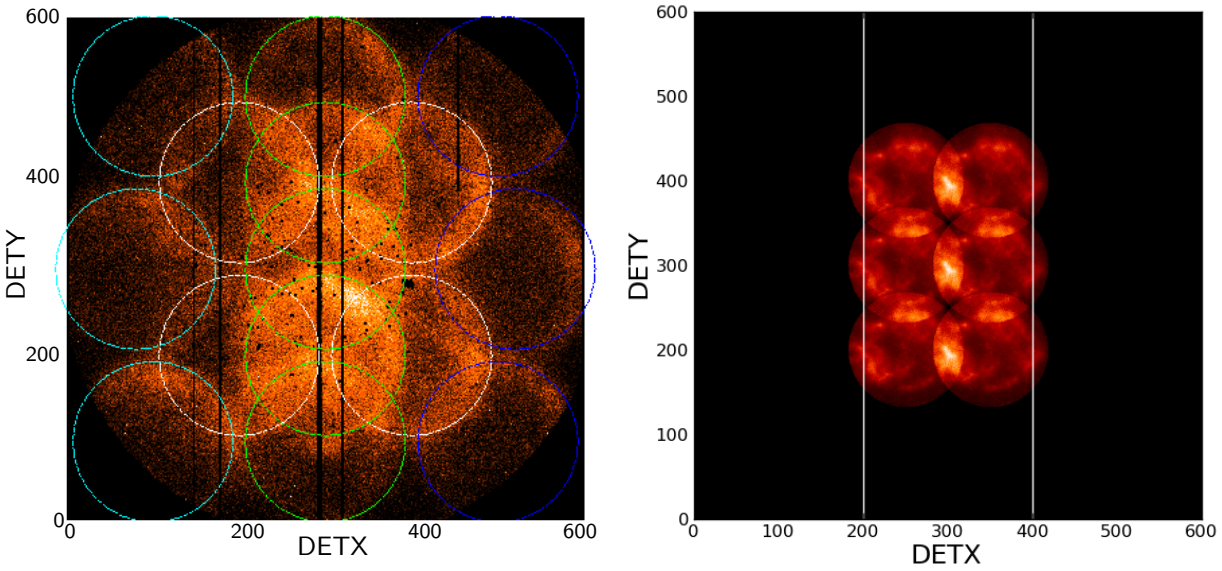

Figure 1: The *left panel* shows the PC trap mapping observing strategy, consisting of 15×20ks pointings covering the entire CCD (in detector coordinates), but biased towards the central 200×400 pixels. The *right panel* illustrates the WT trap mapping strategy, consisting of 6×10ks pointings taken over the central 200×300 pixels.

The previous versions of the gain files (PC – v016; WT – v018), released in May 2017, included updates to the gain and CTI coefficients and trap-depth tables derived from calibration data collected up to the end of October 2016. Due to the incremental nature of the gain file updates, this new gain file release (PC – v017; WT – v019) will only effect the processing of XRT data taken after November 1st 2016.

When XRT data are processed with trap corrections applied (which is the default mode of operation for the XRT software task XRTCALCPI), residual energy scale offsets of $\sim 10 - 20$ eV can sometimes be seen in spectra at energies near $\sim$ 0.5 and $\sim$ 2 keV, which increases to $\sim 30 - 40$ eV at energies close to the iron Kα region (6.4 keV).

The offsets are likely caused by observations whose CCD temperatures are outside the nominal calibrated range of the gain file, or by bright earth contamination. For example, the median CCD temperature for all observations during 2017 (including calibration) was $-58.7°C$, with 90 per cent of the observations spanning the temperature range -63.0 to $-54.0°C$; due to limited data, the energy scale is not as well calibrated for observations taken outside this range, which can lead to energy scale offsets. Also, bright earth contamination causes optical loading in the CCD which can give rise to energy scale offsets. The offsets manifest themselves as $\sim$ 10 per cent residuals around the instrumental edges (e.g. O-K 0.545 keV, Si-K 1.838 keV and Au-M 2.35 keV) in continuum sources with good photon counting statistics. Careful use of the *gain fit* command in XSPEC (allowing *only* the gain offset term to vary) can alleviate these residuals. See also the caveats in Section 3.7.

As the gain files are released approximately yearly and the gain evolution is not extrapolated beyond the last entry in the gain files (2018-May-31), we can expect similar energy scale offsets to develop to those identified above (see paragraph 3 of Section 3.1, above) by January 2019.

Further comments on gain/charge trap corrections (including effects of trailing charge in WT mode) can be found on the *XRT Digest* page (www.swift.ac.uk/analysis/xrt/digest_cal.php) at the UKSSDC.

3.2 Gain files derivation

The gain files include coefficients for the gain and the parallel and serial CTI for different epochs at three reference CCD temperatures (-75C, -61.5C and -48C). The gain coefficients are defined in Appendix A. The coefficients are derived using the ^{55}Fe line in the corner sources spectra at different epochs (Appendix B). Two sets of gain and CTI coefficients are included in the gain files for this release. One set of coefficients, derived from all the events in the corner sources, is used by the software to calculate the event energy when no trap correction is applied. The second set, derived from the columns of the corner sources less affected by charge traps, is used when the traps energy corrections are applied. The CTI energy dependence is modelled with a broken power-law functional form (Appendix A.6).

The gain files format allows for the energy correction for charge trap losses. The traps are identified in the gain files by their locations in detector coordinates (RAWX, RAWY), their extensions in pixels (YEXTENT) and their depths in eV (OFFSET) measured at the incident photons'reference energy of 1856 eV for Tycho, or 1863 eV for Cas A — both of these Silicon Kα line energies were measured from early XMM-Newton MOS1 observations. Starting with the release HEASOFT 6.11, the *Swift* software derives the trap corrected energy and saves it in the *PI* column of the cleaned events files for each valid X-ray event. The temperature dependence of the trap depths has been modelled and the appropriate corrections are included in the PC gain file (Appendix C.4); in WT mode a temperature dependence is not observed because of its faster frame readout time.

3.3 Gain and CTI coefficients

The gain and CTI coefficients are derived using the ^{55}Fe line in the four radioactive corner sources spectra at different epochs (Appendix B). The evolution of the measured line centroids from 2007-Sep-05 to 2018-May-31 at a CCD temperature of -60°C is shown in Figure 2, left panel. The line centroid values are decreasing due to the effects of radiation damage that introduces charge traps in various pixels of the detector. The incremental level of degradation experienced during the last year is similar to that measured in previous epochs.

3.4 Trap corrections

The charge traps generated by radiation damage cause the loss of a fraction of the energy of the detected X-ray events during the signal transfer and readout process (Pagani et al. 2011). The gain files include position-dependent energy offsets ($OFFSET$) to correct for trap losses in individual pixels larger than 20 eV (Appendix A.7). The losses caused by shallower traps are instead modelled and corrected for with the CTI coefficients which apply uniformely for all pixels.

The energy offsets are measured by analysing observations of the Tycho and/or Cas A supernova remnant taken yearly by the *Swift*-XRT calibration team. The details of the trap mapping analysis are described in Appendix C. In this release, new trap offset values were derived for PC mode data using trap mapping observations from August – November 2017, with 15 pointings of the Tycho supernova remnant covering the entire CCD (Figure 1). For WT mode data, 6 offset pointings of Cas A were used to derive energy offsets in December 2017 – January 2018. Trap

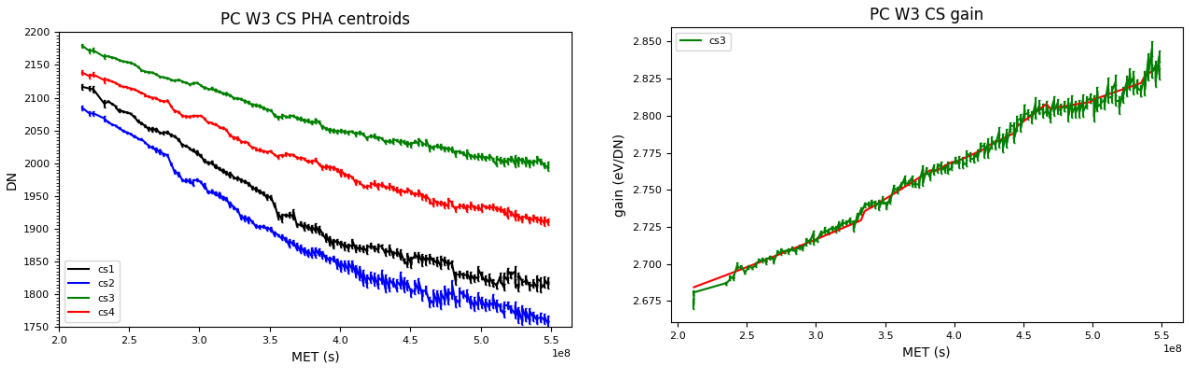

Figure 2: *Swift*-XRT CCD measurements from the corner source data at a CCD temperature of -60°C from 2007-Sep-05 to 2018-May-31. The left panel shows the measured ^{55}Fe line centroids from the four corner sources. The right panel shows the gain coefficient (GC0_TRAP) estimated using equation A.11 from trap free columns used for trap-corrected spectra (in green the measured monthly averaged gain values, in red the modelled gain evolution with time). Error bars are 1σ estimates.

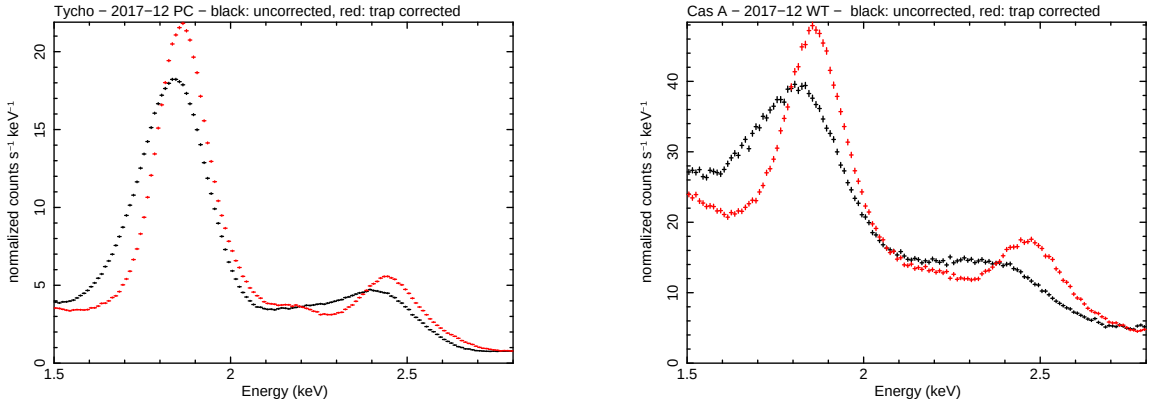

Figure 3: Comparison of non trap corrected spectra (in black) and trap corrected spectra (in red) for Tycho observations taken in PC mode from August – December 2017 (left panel) and Cas A observations taken in WT mode from December 2017 – January 2018 (right panel).

corrections provide a substantial recovery of the emission line flux and the energy resolution in both PC and WT mode, as shown in Figure 3. Tables 2 and 3 present the evolution of the spectral resolution in PC and WT mode derived from Cas A and Tycho observations, illustrating the accumulating radiation damage which gradually degrades the instrument response, and its partial recovery thanks to the application of trap corrections.

3.5 Energy dependence of the trap corrections

The energy dependence of the trap corrections is modelled in the gain files with a broken power law for both PC and WT mode. The Sulphur and Iron Kα lines in Tycho and Cas A observations (E_S = 2450 eV, E_{Fe} = 6440 eV in Tycho, E_S = 2456 eV, E_{Fe} = 6626 eV in Cas A), are used above Silicon (E_{Si} = 1856 eV in Tycho, E_{Si} = 1863 eV in Cas A), and at lower

Table 2: PC mode spectral resolution: Full width half maximum (FWHM) in eV of the Silicon, Sulphur and Iron Kα lines of the observed and the corrected spectra at different calibration epochs (specified as YYYY/MM). The FWHM values at Sulphur and Iron are only reported when enough counts in the lines allow for a reliable fit.

Source	Epoch	Line	$FWHM_{observed}$	$FWHM_{corrected}$
CasA	2007/09	Si	138 ± 7	114 ± 2
		S	200 ± 11	146 ± 6
		Fe	318 ± 22	286 ± 21
CasA	2009/02	Si	154 ± 8	122 ± 2
		S	251 ± 18	163 ± 7
		Fe	372 ± 25	321 ± 14
Tycho	2009/10	Si	179 ± 8	132 ± 3
		S	267 ± 14	182 ± 8
		Fe	381 ± 45	299 ± 31
Tycho	2010/03	Si	177 ± 7	138 ± 3
		S	256 ± 10	184 ± 8
		Fe	381 ± 39	307 ± 32
Tycho	2010/10	Si	192 ± 7	139 ± 7
		S	269 ± 11	192 ± 11
		Fe	387 ± 34	304 ± 27
Tycho	2011/02	Si	185 ± 6	143 ± 7
Tycho	2011/09	Si	191 ± 7	147 ± 7
Tycho	2012/02	Si	191 ± 7	146 ± 7
Tycho	2012/09	Si	198 ± 8	149 ± 7
Tycho	2013/08	Si	206 ± 8	152 ± 7
Tycho	2014/08	Si	216 ± 8	152 ± 7
Tycho	2015/08	Si	213 ± 8	164 ± 7
Tycho	2016/12	Si	218 ± 8	169 ± 7
Tycho	2017/12	Si	217 ± 10	164 ± 5

energies the dependence is derived using the SNRs E0102-72 & N132D and the soft neutron star RX J1856.5-3754 models provided by the International Astronomical Consortium for High Energy Calibration (IACHEC, http://web.mit.edu/iachec/) to fit the spectra of these sources which are measured routinely every 6 months.

The instrumental Nickel Kα line (7470 eV) provides a useful check of the accuracy of the energy dependence at high energies. As can be seen in Figure 4, the Nickel line of the trap corrected data extracted from all the PC observations collected during a given calibration epoch is at the expected energy and presents a recovery in the line flux and resolution compared to non trap-corrected data.

3.6 Temperature dependence of the trap corrections

Tycho SNR PC mode data and the instrumental Nickel Kα line allow us to measure the temperature dependence of the trap corrections (see Section C.4 for more details). In the latest epoch (since March 2016) the observed dependence has been corrected for by introducing energy

scale offsets (GC3_TRAP) and distinct trap offsets at three reference CCD temperatures (-75C, -61.5C and -48C) in the PC gain file. The XRT data reduction software calculates and applies the appropriate energy offset by interpolating between the reference offsets included in the gain file. The results of the applied corrections for the Tycho and Nickel 2016 datasets can be seen in the right panels of Figure 5. A temperature dependence is not observed in WT mode data because of its faster readout mode.

3.7 Limitations in the current release

Some limitations remain in the current release.

- The accuracy of the trap mapping measurements in PC mode data is dependent on the statistics of the reference Silicon Kα line, and only traps with a depth greater than 20 eV can be identified;
- With the current release we keep improving on the uniformity of the spectral energy response in PC mode across the detector, thanks to the more uniform coverage of the CCD achieved with the latest observation strategy. The trap mapping analysis in regions with poor coverage only allows the determination of the trap location with an accuracy of ~ 5 pixels because of the lower Silicon line photon statistics; the trap positions will be

Table 3: WT mode spectral resolution: Full width half maximum (FWHM) in eV of the Silicon, Sulphur and Iron Kα in the observed and the the corrected spectra for different calibration epochs (specified as YYYY/MM). The FWHM values at Sulphur and Iron are only reported when enough counts in the lines allow for a reliable fit.

Source	Epoch	Line	$FWHM_{observed}$	$FWHM_{corrected}$
CasA	2007/10	Si	152 ± 13	106 ± 3
		S	244 ± 15	138 ± 7
		Fe	383 ± 16	304 ± 15
CasA	2008/07	Si	157 ± 14	113 ± 4
		S	274 ± 17	154 ± 9
		Fe	393 ± 22	325 ± 17
CasA	2009/10	Si	212 ± 16	120 ± 3
		S	302 ± 11	170 ± 11
Tycho	2009/11	Si	222 ± 15	136 ± 7
Tycho	2010/10	Si	238 ± 12	148 ± 5
Tycho	2011/02	Si	234 ± 11	150 ± 6
Tycho	2011/08	Si	234 ± 12	154 ± 6
Tycho	2012/02	Si	243 ± 12	160 ± 7
Tycho	2012/08	Si	249 ± 12	166 ± 7
Tycho	2013/08	Si	270 ± 12	168 ± 7
Cas A	2014/08	Si	263 ± 12	157 ± 8
Cas A	2015/08	Si	293 ± 12	162 ± 8
Cas A	2016/12	Si	313 ± 12	169 ± 8
Cas A	2017/12	Si	275 ± 25	173 ± 5

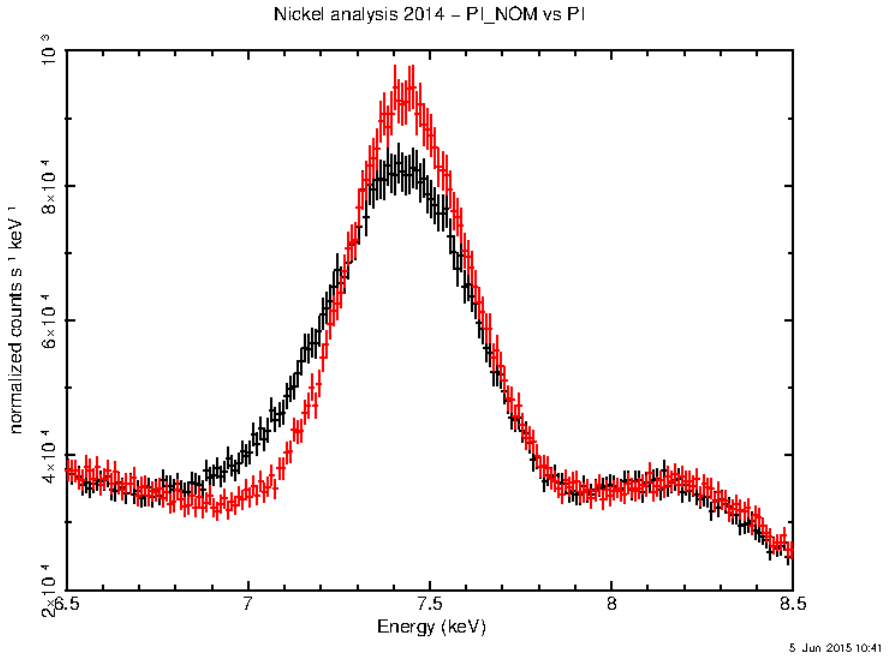

Figure 4: Nickel line extracted from PC observations collected between August 2014 and December 2015 with exposure greater than 100 seconds, to illustrate the trap corrections at high energies. The trap corrected spectrum (in red) shows a recovery of the line flux and an improvement of the energy resolution in comparison to the observed spectrum (in black).

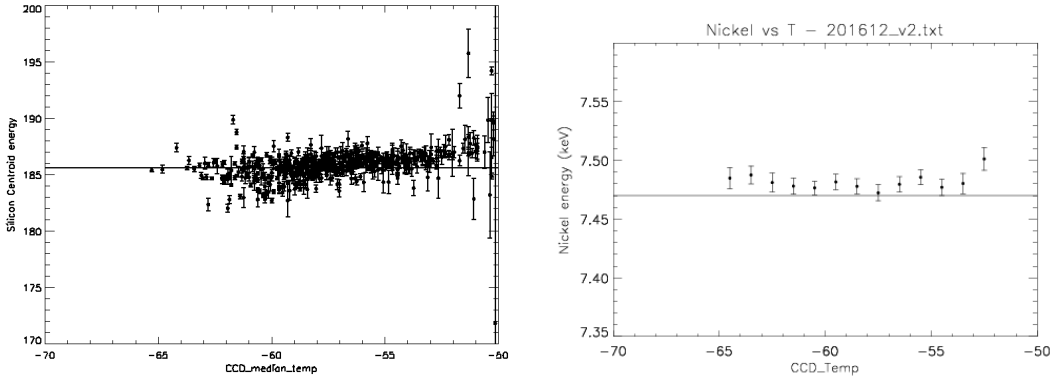

Figure 5: After processing the data with the revision 17 gain file (swxpcgains6_20010101v016.fits), the Gaussian fits to both the Silicon line in Tycho (left panel) and the instrumental Nickel Kα line (right panel) are close to the expected values at all temperatures.

refined as additional observations from future calibration epochs will be merged with the current datasets;

- In WT mode observations, traps are not mapped individually, and only the cumulative energy offsets of fixed segments along the columns is measured and corrected;
- In datasets affected by scattered light from the sunlit Earth (Bright Earth contamination) the optical photons can fill the charge traps and cause spectral shifts to higher energies; in the worst cases, with observations taken at temperatures above -55 C, shifts in the energy lines up to $\sim$ 50 eV have been measured. With a change in observation strategy (in 2016), and new guidelines to limit the temperature range, we have minimised these

effects, but it is not possible to completely avoid them;

- In between releases of updated gain files new traps caused by radiation damage will develop that can cause shifts in the measured energies that depend on the observed source positions on the detector. The changes in the observation strategy allow us to better monitor the appearance of new traps, but the change to a yearly, rather than twice yearly, release strategy will worsen the effect of the energy losses between gain file releases.
- The gain correction software XRTCALCPI interpolates the gain coefficients between 3 temperatures (-75C, -61.5C and -48C), originally choosen to match the spread in temperatures from the corner source calibration data taken in ∼2008–2012. Due to spacecraft operational constraints, the majority of observations are now performed over show a much narrower range in CCD temperatures (e.g. in 2017 the median temperature was -58.7C, with 90 per cent of observations occuring between -63C to -54C). This means the gain coefficients at the higher and lower temperature extremes suffer from extrapolation uncertainties leading to energy scale offsets. For example, recent (2018-June) safepointing observations taken at -70C in PC mode have shown energy scale offsets of order 100 eV (to higher energies). This will be improved in future releases of the gain file.

Because of the above limitations and the pixel-specific nature of the distribution of traps on the detector, a general description of the accuracy of the XRT energy scale for this gain file calibration release is not straightforward. We estimate the accuracy by fitting short observations of the Cas A SNR taken months after the trap-mapping calibration epochs using XMM derived models. When the line energies are left as free parameters, differences of less than 20 eV from the XMM values are measured in the PC spectrum, while in WT mode the differences can be higher, up to 30 eV at Iron Kα. The Leicester calibration team maintains an *XRT Digest* page (www.swift.ac.uk/analysis/xrt/digest_cal.php) at the UKSSDC with up-to-date information on the XRT calibration status and the known issues.

3.8 Revision 18 gain release and RMF/ARF combination

The gain files released in this CALDB update, suitable for substrate voltage $V_{ss} = 6\,\mathrm{V}$ data[a] are: **swxpcgains6_20010101v017.fits** for Photon Counting mode and **swxwtgains6_20010101-v019.fits** for Windowed Timing mode. Spectra extracted using the new gain files should be fitted with the **swxs6_20010101v001.arf** ARF file and with the RMF file chosen depending on the epoch of the observations (Beardmore et al. 2013, Beardmore et al. 2014).

4 Review of Previous Gain File Changes

This section reviews the prior history of the gain file before this release.

[a] All data after 2007-Aug-30, 14:25UT, have been taken with $V_{ss} = 6\,\mathrm{V}$, when the substrate voltage was raised permanently.

4.1 Passive cooling and Substrate Voltage change

The loss of the CCD active cooling system shortly after launch forced the instrument to rely on passive cooling provided by the XRT radiator in order to operate the detector in the -75°C to -50°C temperature range rather than the -100°C envisaged before launch. The main effects of operating at such temperatures is a change of gain and a significant level of dark current and elevated CCD noise at low energies, with an increasing number of hot and 'flickering' pixels at higher temperatures.

On 2007-Aug-30 at 14:25UT, the XRT team performed a planned substrate voltage (V_{ss}) change from 0 V to 6 V in order to reduce the thermally induced dark current when the operating temperature is above -55 °C. Prior to the change, preliminary observations of Cas A and the Crab at a V_{ss} of 6 V showed a reduction in the Quantum Efficiency of the order of 10% at 6 keV (Godet et al. 2007, SPIE, 6686) and an increase of about 5% in the gain due to the change in the gain of the output FET. The latter meant separate gain files are needed depending on the substrate voltage at the time of a given observation. The files are distinguished using the notation *s0* (for $V_{ss} = 0$ V) and *s6* (for $V_{ss} = 6$ V) in their respective file names. The *Swift* software tools (version 2.3 and onwards) were updated to perform a query for the relevant gain file to be used depending on the substrate voltage setting.

4.2 Radiation damage

Radiation damage during the orbital lifetime of *Swift* continues to degrade the XRT CCD camera performance. The interaction of soft and hard protons with the CCD produces displacements of Silicon atoms that cause charge traps in its crystal lattice, resulting in offsets in the measured photons energies and in the broadening of the spectroscopic resolution.

In September of 2007 the XRT team started a calibration program to characterise the charge losses due to traps consisting of observations of the emission line rich Cas A and Tycho Supernova Remnants (SNRs). In Photon Counting (PC) mode, the locations of the deeper traps and their depths are measured in the central 200x200 pixels of the CCD. Outside the central window, the cumulative effects of traps are evaluated for individual CCD column. Column energy offsets are also evaluated in Windowed Timing (WT) mode, that provides high time resolution with 1-D spatial localisation. The observations of the SNRs are repeated approximately every six months, and updated trap tables are derived. The CALDB gain files in this release have been updated including trap tables from 2 additional epochs (February and August-September 2012) as derived from observations of the Tycho SNR. The temperature dependence of the trap depths was also characterized and updated gain coefficients were included in this release.

The XRTCALCPI software task implements the energy corrections for charge traps and the CTI energy dependence. The software automatically applies the appropriate gain corrections dependent on the time of observation, CCD temperature and event position. The trap mapping analysis is described in Appendix C.

4.3 Calibration corner source analysis and CTI energy dependence

In 2008 June, after successful XRT flight software updates, the XRT CCD began permanently operating in full frame PC mode ('pcw3'), whereby the entire 600×600 imaging area of the CCD is read out. This has enabled us to continuously collect corner source ^{55}Fe calibration data (see figure A.1) when operating in PC mode and has provided us with a wealth of information on the gain and charge transfer efficiency (CTE) behaviour as a function of time and CCD temperature since this time.

Moreover, analysis of the corner source data and measurements of the nickel background line in addition to the Tycho, Cas A and E0101 SNR lines has clearly shown that the CTI correction should be energy dependent. The energy dependence (coefficients GC1, GC2 and GC1_TRAP, GC2_TRAP of the gain files) has been calibrated and modelled with a broken power law and implemented in the XRTDAS software version 2.8.0 and onwards. The 'Calibration Dataset Codename', used by the software to query the CALDB has been set to 'GAIN2' in the gain files with the new CTI energy dependence:

CCNM0001= 'GAIN2 ' / Type of Calibration data

This setting prevents the software from using an incorrect version of the gain files.

APPENDIX

A Gain and CTI coefficients

A.1 Introduction

The charge transfer efficiency (CTE) is defined as the fractional charge lost per pixel during the charge transfer process. So after N transfers the remaining charge Q is

$$Q = Q_o(CTE)^N \tag{A.1}$$

where Q_o is the initial charge. Or in terms of charge transfer inefficiency $CTI = 1 - CTE$ this is just

$$Q = Q_o(1 - CTI)^N \tag{A.2}$$

A.2 Event energy measured in the Swift-XRT CCD22

A schematic of the *Swift*-XRT CCD22 is showed in figure A.1. When an incident X-ray of energy E is registered as an event at a detector position (X, Y) in the image section it suffers charge loss from Y transfers in the parallel direction through the image section, from $Y_S = 600$ transfers in the parallel direction through the frame-store section and from $X + 5$ transfers in the serial direction through the readout register (+5 as there are 5 additional pixels at the end of the readout register). CTI values differ in the parallel and serial direction because of the different transfer times and pixel sizes. In order to describe the total charge lost effectively we

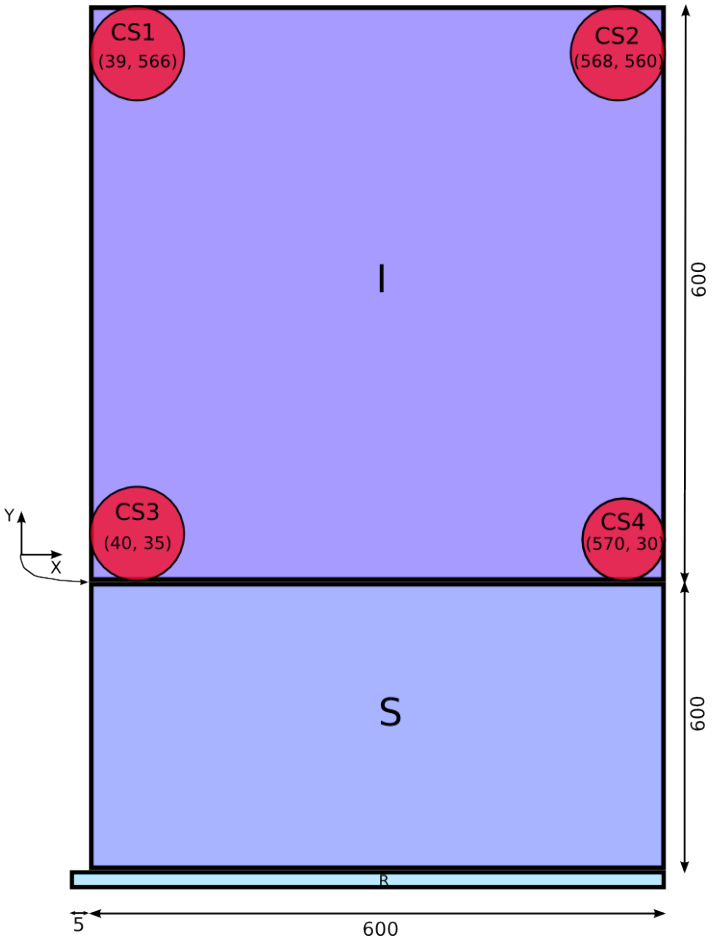

Figure A.1: Schematic of the *Swift*-XRT CCD22 identifying the imaging (I) and frame-store (S) sections, the readout register (R), and the ^{55}Fe corner sources (CS). Charged is clocked in the parallel direction (Y), through both the imaging and frame-store sections, which have charge transfer inefficiencies $CTI_{p,i}$ and $CTI_{p,f}$, respectively, and in the serial direction through the readout register with CTI_s.

need separate CTI coefficients for the parallel transfer losses incurred in the image and frame-store sections ($CTI_{p,i}$ and $CTI_{p,f}$, respectively, as the physical volume of the pixels are smaller in the latter compared with the former) and another for the serial transfer losses (CTI_s).

The event is registered by the ADC as a pulse-height analysed digital number D (i.e. the PHA value) according to the following:

$$D = \frac{E}{A}(1 - CTI_{p,i})^{Y}(1 - CTI_{p,f})^{Y_S}(1 - CTI_s)^{(X+5)} \tag{A.3}$$

Or rearranging slightly, this becomes

$$\begin{aligned} D &= E\left[\frac{(1 - CTI_{p,f})^{Y_S}(1 - CTI_s)^5}{A}\right](1 - CTI_{p,i})^{Y}(1 - CTI_s)^{X} \\ &= \frac{E}{A'}(1 - CTI_{p,i})^{Y}(1 - CTI_s)^{X} \end{aligned} \tag{A.4}$$

where $A' = A/((1 - CTI_{p,f})^{Y_S}(1 - CTI_s)^5$ is the system gain.

A.3 CTI coefficients

The parallel CTI can be determined from CS3 and CS1 by using equation A.4 to construct the ratio $(D_3 - D_1)/D_3$, where D_n are the measured ^{55}Fe central energies (in DN) for source $n = 1 \ldots 4$, which is

$$\begin{aligned} \frac{D_3 - D_1}{D_3} &= \frac{(1 - CTI_{p,i})^{Y_3}(1 - CTI_s)^{X_3} - (1 - CTI_{p,i})^{Y_1}(1 - CTI_s)^{X_1}}{(1 - CTI_{p,i})^{Y_3}(1 - CTI_s)^{X_3}} \\ &= 1 - (1 - CTI_{p,i})^{(Y_1 - Y_3)}(1 - CTI_s)^{(X_1 - X_3)} \quad \text{(A.5)} \\ &= 1 - (1 - CTI_{p,i})^{(Y_1 - Y_3)} \quad \text{(A.6)} \end{aligned}$$

where equation A.6 is a simplification assuming $X_1 \approx X_3$ for transfers dominating in the parallel direction (i.e. $Y_1 - Y_3 \gg X_1 - X_3$). Rearranging we find

$$CTI_{p,i} = 1 - \left(\frac{D_1}{D_3}\right)^{1/(Y_1 - Y_3)} \quad \text{(A.7)}$$

We often make use of the small number approximation (i.e. $(1 + x)^n \approx 1 + nx$) so equation A.6 becomes

$$\frac{D_3 - D_1}{D_3} = (Y_1 - Y_3)CTI_{p,i}$$

That is, the parallel CTI is

$$CTI_{p,i} = \frac{D_3 - D_1}{D_3(Y_1 - Y_3)} \quad \text{(A.8)}$$

A similar equation can be derived for the parallel CTI derived from CS4 and CS2.

Likewise, the serial CTI can be shown to be

$$\begin{aligned} CTI_s &= 1 - \left(\frac{D_4}{D_3}\right)^{1/(X_4 - X_3)} \quad \text{(A.9)} \\ &= \frac{D_3 - D_4}{D_3(X_4 - X_3)} \quad \text{(A.10)} \end{aligned}$$

A.4 Gain

We can obtain the gain A' from CS3, which is the corner source closest to the output amplifier,

$$A' = \frac{E_{^{55}\mathrm{Fe}}}{D_3}(1 - CTI_{p,i})^{Y_3}(1 - CTI_s)^{X_3} \quad \text{(A.11)}$$

where $E_{^{55}\mathrm{Fe}} = 5895.45\,\mathrm{eV}$, $X_3 = 40$ and $Y_3 = 35$. Note the term $(1 - CTI_{p,i})^{Y_3}(1 - CTI_s)^{X_3}$ which provides a small correction to the simple gain estimate of $E_{^{55}\mathrm{Fe}}/D_3$ and ensures the event energy is calculated relative to the origin $(0, 0)$ of the imaging section of the CCD.

A.5 Comparison with the CALDB gain file

The CALDB gain file defines the PHA channel to PI channel conversion as

$$PI \times G = PHA\,(GC0 + X \times GC1 + Y \times GC2) + GC3 + X \times GC4 + Y \times GC5 \qquad \text{(A.12)}$$

where GCn are the gain file coefficients (which are interpolated over time and CCD temperature), and $G = 10\,\mathrm{eV}$ is the nominal gain.

Equation A.4 can be rearranged to give the event energy from the measured DN value, assuming the CTI coefficients are known,

$$E = A'\,D\,(1 - CTI_{p,i})^{-Y}\,(1 - CTI_s)^{-X}. \qquad \text{(A.13)}$$

Note, this is the exact form of the equation required to reconstruct the event energy from the measure DN value, knowing the gain (A') and CTI values.

This equation can be made to resemble the CALDB formula by using the small value approximation expansion :

$$\begin{aligned} E &= A'\,D\,(1 + Y\,CTI_{p,i})\,(1 + X\,CTI_s) \\ &= A'\,D\,(1 + X\,CTI_s + Y\,CTI_{p,i} + X\,Y\,CTI_s\,CTI_{p,i}) \end{aligned}$$

and dropping the last negligibly small term to give

$$\begin{aligned} E &= A'\,D\,(1 + X\,CTI_s + Y\,CTI_{p,i}) \\ &= D\,\{A' + X\,(A'\,CTI_s) + Y\,(A'\,CTI_{p,i})\}. \end{aligned} \qquad \text{(A.14)}$$

By comparison with equation A.12, we see that

$$\begin{aligned} GC0 &= A' \\ GC1 &= A'\,CTI_s \\ GC2 &= A'\,CTI_{p,i} \end{aligned} \qquad \text{(A.15)}$$

In practise, CTI_s is estimated from corner sources CS3–CS4, while $CTI_{p,i}$ is estimated as the average parallel CTI from corner sources CS1–CS3 and CS2–CS4.

The term $GC3$ in equation A.12 represents an offset (in eV) associated with the readout electronics.

A.6 CTI coefficients energy dependence

Laboratory experiments and various X-ray missions (e.g. Chandra, Suzaku) indicate that CTI is energy dependent. We choose to implement an energy dependent CTI correction as a broken power law with index $\beta 1$ and $\beta 2$ below and above the break energy:

$$\begin{aligned} CTI(E) &= CTI(E_{^{55}\mathrm{Fe}})(\frac{E}{E_{^{55}\mathrm{Fe}}})^{-\beta 1} \qquad (E \le E_{^{55}\mathrm{Fe}}) \\ &= CTI(E_{^{55}\mathrm{Fe}})(\frac{E}{E_{^{55}\mathrm{Fe}}})^{-\beta 2} \qquad (E > E_{^{55}\mathrm{Fe}}) \end{aligned} \qquad \text{(A.16)}$$

with $E_{^{55}\mathrm{Fe}} = 5.895\,\mathrm{keV}$ and $\beta > 0$.

The CTI energy dependence parameters in the CALDB gain files are labelled as BETA1, BETA2 and E_CTI.

A.7 Trap correction coefficients

The trap corrections are implemented in the gain files using an additive offset coefficient to equation A.12:

$$PI \times G = PHA\,(GC0 + X \times GC1 + Y \times GC2) + GC3 + X \times GC4 + Y \times GC5 + OFFSET \quad \text{(A.17)}$$

The OFFSET coefficient is added to the $PI \times G$ values of events detected at specific CCD locations affected by charge traps. In the gain files, the trap positions are labelled as RAWX, RAWY and YEXTENT, such that the OFFSET PI value will be added to events along the CCD column RAWX between rows RAWY and RAWY+YEXTENT.

The trap offset energy dependence is modelled with a broken power law, with the break at the reference energy of 1.856 keV(the energy of the Silicon Kα line of the Tycho SNR):

$$\begin{aligned} \mathrm{Offset(E)} &= \mathrm{Offset(E_{break})}\left(\frac{\mathrm{E}}{\mathrm{E_{break}}}\right)^{\alpha 1} \qquad (\mathrm{E} \leq \mathrm{E_{break}}) \\ &= \mathrm{Offset(E_{break})}\left(\frac{\mathrm{E}}{\mathrm{E_{break}}}\right)^{\alpha 2} \qquad (\mathrm{E} > \mathrm{E_{break}}) \end{aligned} \quad \text{(A.18)}$$

The offsets energy dependence parameters in the CALDB gain files are labelled as ALPHA1, ALPHA2 and EBREAK. The gain and CTI coefficients and the energy dependence parameters used by the software to compute trap corrected events energy are labelled as GC0_TRAP, GC1_TRAP, GC2_TRAP, GC3_TRAP, GC4_TRAP, GC5_TRAP, BETA1_TRAP, BETA2_TRAP and E_CTI_TRAP.

B Gain and CTI measurements

B.1 Corner source data analysis

Gain and CTI coefficients are measured from the analysis of the corner source data. A first set of coefficients is derived using the entire dataset, and characterises the CCD response when trap energy corrections are not applied. A second set of coefficients, derived from corner source data least affected by traps, models the gain and the CTI of trap-corrected spectra. For both derivations, the same procedure is applied and is described below.

The corner source are processed applying the PC mode bias corrections. Grade 0 PHA spectra

are extracted from each of the corner sources as a function of time and CCD temperature. The spectra near the ^{55}Fe line are then fit with the following asymmetric Gaussian function :

$$\begin{aligned} G(x) &= N \exp\left(-0.5\left(\frac{x-x_c}{\sigma_1}\right)^2\right) \qquad (x < x_c) \\ &= N \exp\left(-0.5\left(\frac{x-x_c}{\sigma_2}\right)^2\right) \qquad (x > x_c) \end{aligned}$$

where x_c is the line centre, σ_1 the line width for $x < x_c$, σ_2 the line width for $x > x_c$, and N the normalisation. This models the line profile better and returns more accurate line centroids than a simple Gaussian, as the effect of CTI is to broaden the low energy line wing significantly more than the high energy line wing (Godet et al. 2009, A&A, 494, 775).

B.1.1 Gain and CTI coefficients for non trap-corrected spectra

Figure B.2 illustrates the measured line centroids, gain and CTI coefficients from 2007-Sep-05 to 2016-Nov-01 at a CCD temperature of -60C when all the corner source data is used (i.e., without excluding traps).

Due to the excellent quantity and statistical quality of the corner source data obtained since 2008-June we have been able to study and quantify the measured gain and CTI coefficients behaviour as a function of time and CCD temperature. Figure B.3 shows the gain (GC0) and CTI coefficients (GC1,2) derived from the entire corner source dataset, plotted as a function of CCD temperature at 4 representative epochs. The data reveal the gain has evolved to become less sensitive to the CCD temperature, while the parallel CTI decreases with increasing temperature and the serial CTI increases slightly with temperature.

We have parameterised the gain and CTI time (t) and CCD temperature (T) dependence using the following functional form :

$$z(t,T) = a + b\,t + c\,T + d\,t^2 + e\,T^2 + f\,t\,T.$$

The model curves are shown plotted with the data in figure B.3.

The parameterised GC0, GC1 and GC2 (see equation A.12) values derived from non trap-corrected data were then converted into a template gain file with coefficients calculated at monthly intervals and at three discrete temperatures (-73, -60.5, -48$^{\circ}C$). The *Swift*-XRT software task XRTCALPI interpolates over time and temperature when applying the gain calculation to the event data.

The template gain file for non trap-corrected data was tested on various data sets which included the corner source data (PC mode) and the line rich SNRs E0102 and Cas A (both PC and WT mode). The low energy spectrum of SNR E0102, in particular, is sensitive to the presence of residual offsets in the energy scale. This is due to the presence of traps that causes energy offsets of the observed energies.

PC mode calibration observations of E0102 taken between 2007 to 2012 revealed the need for an additional offset for non trap-corrected spectra. The offset is modelled as a function of

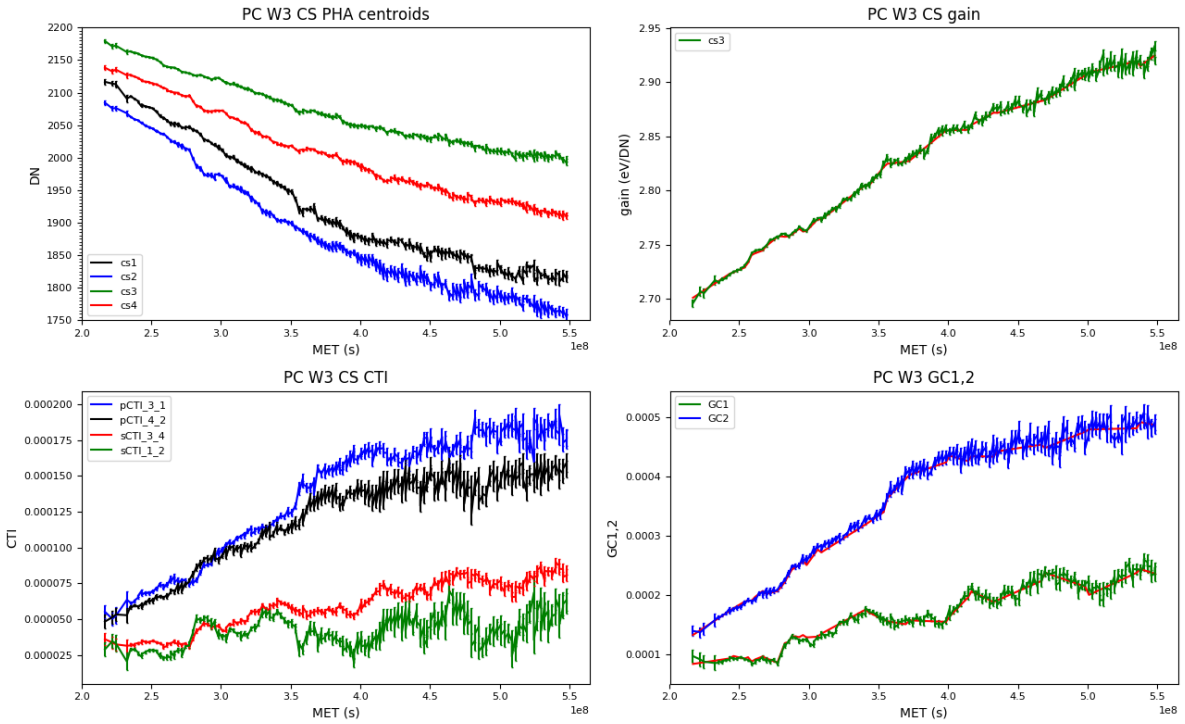

Figure B.2: *Swift*-XRT CCD gain and CTI measurements from the corner source data at a CCD temperature of -60C from 2007-Sep-05 to 2018-May-31. No trap-correction has been applied to the data – i.e. the GCn coefficients correspond to the PI_NOM energy scale. The top-left panel shows the measured ^{55}Fe line centroids. The top-right panel shows the gain coefficient ($GC0$) estimated using equation A.11. The bottom-left panel shows the measured CTI coefficients for the 4 pairs of corner sources. The bottom-right panel shows the estimated gain file $GC1$ (serial) and $GC2$ (parallel) coefficients. (Error bars are 1σ estimates.) The magenta curves overlaid on the data in the top right and bottom right panels show the modelled coefficients as included in the gain file.

time with a linear fit and included in the gain file as the GC3 coefficient. At present, we have no independent measure of the CTI characterisation in WT mode so use the PC mode CTI coefficients in the construction of the WT gain file. Like PC mode, we checked the residual offset using observations of E0102 taken between 2007 and 2012. These showed an average offset of 40 eV valid for all epochs and included as the GC3 coefficient in the gain files.

B.1.2 Gain and CTI coefficients for trap-corrected spectra

The analysis of the corner source data have revealed an ever increasing number of deep traps (20 eV or deeper) in the XRT camera. Because these deep traps were not excluded from the corner source analysis, the gain and CTI coefficients measured as described above are representative of a CCD response with no trap corrections applied and are labelled in the gain files as GC0, GC1, GC2 and GC3.

To characterise the gain and the CTI of trap-corrected spectra a subset of the corner source columns was selected. As the energy offsets of the deeper traps (> 20 eV) are corrected by the software the gain and the residual CTI is best described by the columns least affected by traps. In particular, the columns within 50 eV of the highest measured ^{55}Fe energy centroid in the

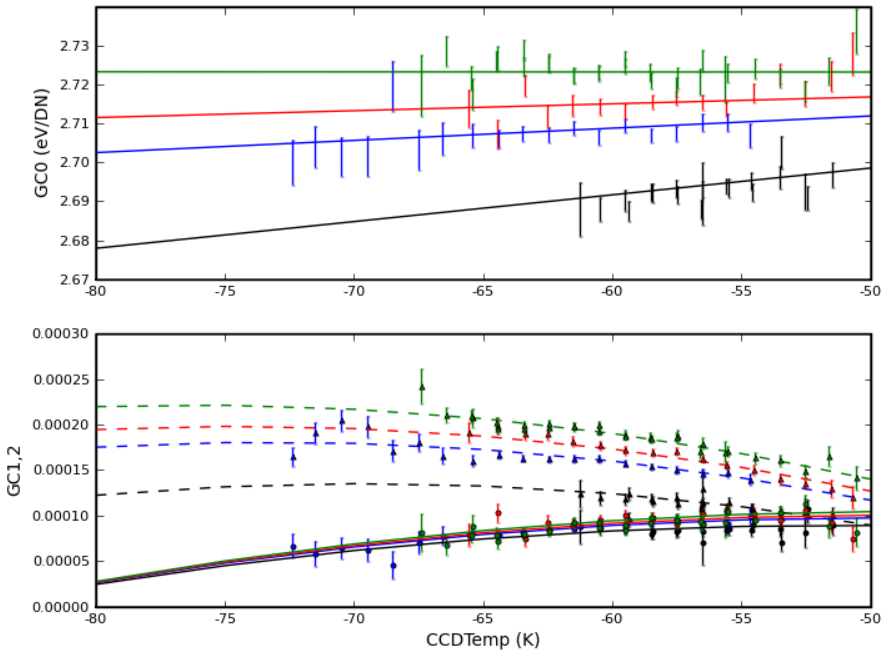

Figure B.3: *Swift*-XRT CCD gain (GC0) and CTI (GC1,2) coefficients plotted against CCD temperature. The model described in the text is over-plotted as the curved lines. For both panels the colour coding is a follows : black – 2007-Sep-06; blue – 2008-Jun-07; red – 2008-Sep-15; green – 2008-Jan-25. In the lower panel, the GC1 (serial) values are drawn as circles and the model is represented by the solid curves, while the GC2 (parallel) values are drawn as triangles and the model curves are shown dashed.

bottom left corner source (DETX = 13, 17, 22, 41) were used to derive the gain coefficient. For the parallel CTI, the accepted columns had a centroid difference in the top and the bottom corner sources within ±2 PI channels (± 25 eV) of each other: DETX = 6, 9, 13, 20, 23, 31, 36, 47, 57, 67, 68, 69 on the left side of the CCD; DETX = 539, 542, 548, 550, 558, 574, 578, 588, 596, 598 on the right side of the CCD. As already mentioned, the serial CTI for trap corrected spectra is set to zero in the CALDB files, as global energy offsets for each CCD column are instead measured and included in the gain file; for this same reason, GC3_TRAP is also zero in the gain files.

The coefficients used by the software task XRTCALPI when the trap correction is applied are labelled as GC0_TRAP, GC1_TRAP, GC2_TRAP and GC3_TRAP. The coefficients are parametrised as a function of time and CCD temperature with the same functional form used for the gain and CTI coefficients of uncorrected spectra previously described.

C Trap mapping

The extreme *Swift* environment, and in particular the transits through the South Atlantic Anomaly, have caused a substantial degradation of the CCD performance, mostly due to the creation of charge traps. Figure C.4 shows the comparison of the Cas A SNR spectrum at launch and in an uncorrected observation taken in 2010. The energy degradation is severe,

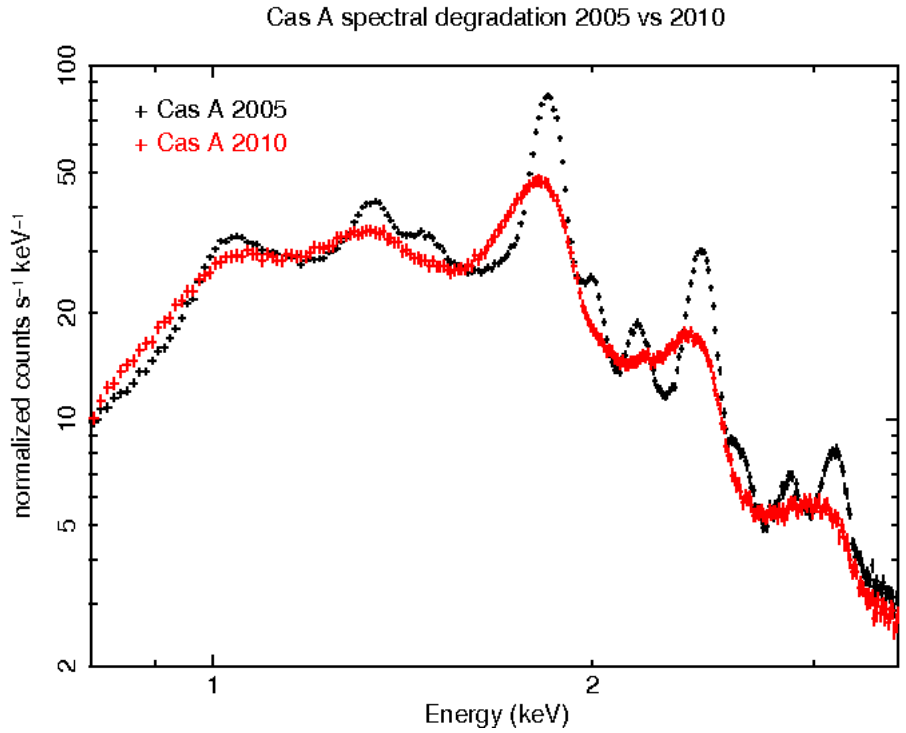

Figure C.4: Comparison of the Windowed Timing mode Cas A spectrum at launch and in a 2010 observation, showing the reduced energy resolution that causes the broadening of the brighter lines of the remnant and the complete disappearance of the weaker lines. The fit of the Silicon K α line with an asymmetric Gaussian in IDL yielded an FWHM of 103 ± 3 eV and of 259 ± 37 eV, in the 2005 and 2010 dataset respectively.

causing the broadening of the brighter lines and the disappearance of the weaker ones.

The initial approach in dealing with the spectral degradation had been the application of a broadening function to the original spectral response (Godet et al. 2009). Using this technique the XRT team generated and released RMFs[b] with a redistribution function which matches the broadened response kernel of the detector at any time. As the spectral resolution continued to worsen, this temporary fix was replaced by the better approach of mapping the locations and depths of the traps and correcting the event data for the energy losses incurred (Pagani et al. 2011). The benefit of this method is that it can restore the spectral resolution of the CCD to something approaching its value at launch.

C.1 Photon Counting mode trap mapping

In Photon Counting mode traps are mapped in the central 200x200 pixels window of the CCD, where most of the GRB afterglows and other astrophysical X-ray sources are observed by the XRT. The exact trap localisation ideally requires the collection of enough source events to fit the

[b]Two sets of WT and PC RMFs including an epoch-dependent broadened kernel have been released: the first set should be used for data collected from 2007 March 1 to 2007 August 31 (**swxpc0to12s0_20070301v011.rmf** & **swxpc0s0_20070301v011.rmf** for PC mode and **swxwt0s0_20070301v011.rmf** & **swxwt0to2s0_20070301v011.rmf** for WT mode) the second set from 2007 September 01 onwards (**swxpc0to12s6_20070901v011.rmf** & **swxpc0s6_20070901v011.rmf** for PC mode and **swxwt0s6_20070901v012.rmf** & **swxwt0to2s6_20070901v012.rmf** for WT mode)

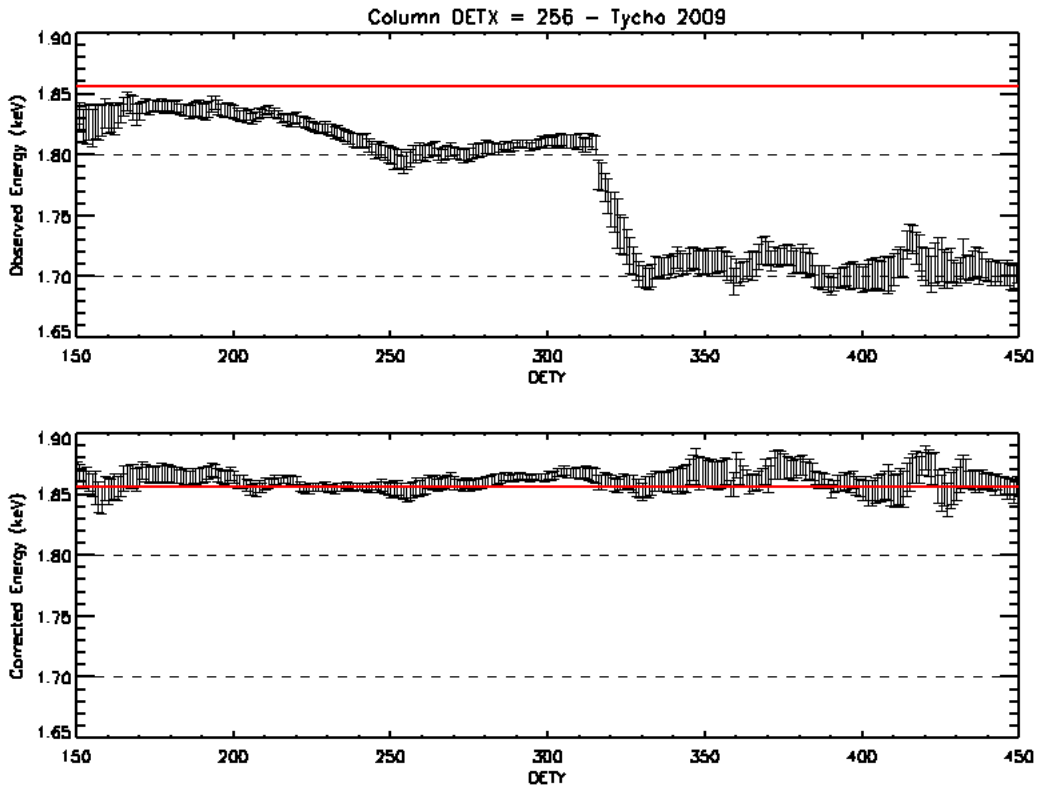

Figure C.5: In the top plot, a deep trap is identified in a Cas A Photon Counting mode observation in CCD column DETX=256 at DETY $\sim$ 310; in the bottom plot, the Si-Kα line energy is restored after the trap correction has been applied.

Si-Kα line with a Gaussian for each CCD pixel. This isn't feasible, as it would greatly exceed the allocated calibration observing time of the *Swift* mission. In practice, the exposure times of the Cas A and Tycho calibration observations are sufficient to obtain an acceptable Gaussian fit of the Si-Kα line from the merging of events of 20 adjacent pixels. Software tools have been developed to fit the Si-Kα line along the CCD columns, to localise traps and measure their depths. An example of trap mapping and correction is shown in Figure C.5. A trap $\simeq$ 100 eV deep is localised in Column DETX = 256, at the approximate row coordinate DETY = 310. In the top plot, each datapoint is the energy centroid of the Gaussian fit of events collected in the 20 pixels above the DETY row coordinate. The line centroid energy after the correction for trap losses has been applied is shown in the bottom plot. This technique allows the identification of traps with a depth of 20 eV or larger.

Figure C.6 is the comparison of the spectrum of the Tycho remnant observed in October 2009 and the spectrum after the correction for traps has been applied, showing an evident recovery of the spectral lines and of the energy resolution. To quantify the improvement in resolution the Si-Kα, S-Kα and Fe-Kα lines of the observed and the corrected spectra of different calibration epochs were fitted in IDL with a modified Gaussian ($f \propto e^{\frac{(x-E)^2}{2\sigma 1^2}}$ for x $\geq$ E, $f \propto e^{\frac{(x-E)^2}{2\sigma 2^2}}$ for x $<$ E), needed to model the asymmetric distortion of the spectral lines caused by trap losses. The results are reported in Table 2.

Trap mapping of the central window of the CCD requires a substantial investment of observing time. Outside the central 200x200 pixels, to keep the exposure time within the allocated calibration time budget, shorter observations of the SNRs are collected, allowing the measurement

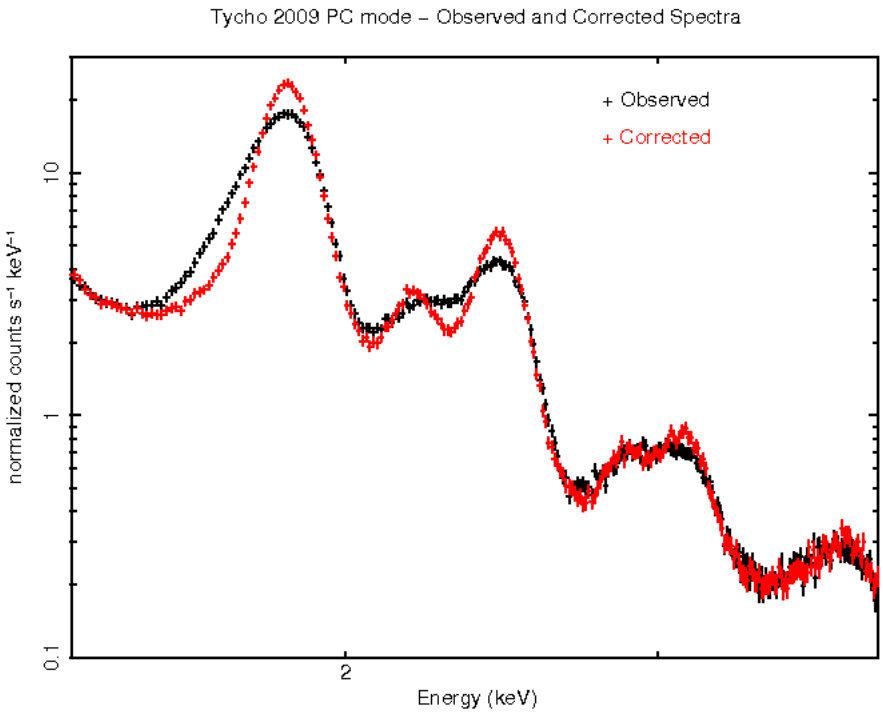

Figure C.6: Comparison of the observed and the trap corrected spectra extracted from a PC mode observation of the Tycho SNR from October 2009. The fit of the Silicon Kα line with an asymmetric Gaussian in IDL yielded a FWHM of 179 ± 8 eV for the observed spectrum and of 132 ± 3 eV for the corrected spectrum.

of the cumulative charge losses due to traps in specific columns (column energy offsets). This approach, that doesn't localise and correct for the charge losses of individually trapped pixels, provides nevertheless a considerable improvement of the energy resolution.

The serial CTI coefficient is defined as the fraction of charge lost per pixel during serial transfers, when the charge is readout in the serial register to the output amplifier. In reality, the CTI is not uniform over the detector because of the non-uniform distribution of traps. The measurement of the columns energy offsets is in effect a more precise characterisation of the serial charge losses than the CTI coefficient, because it evaluates the charge lost for each column. Hence, the serial CTI coefficient GC1_TRAP has been set to zero in the current release.

C.2 Windowed Timing mode trap mapping

Windowed Timing mode provides high time resolution with 1-D spatial localisation, therefore it is not possible to measure the row coordinates and depths of single traps. For this reason, global energy offsets from the reference Si-Kα line are measured on a column by column basis, as in PC observations outside the central 200x200 pixels window.

The *Swift-XRT* pipeline can estimate the *average* row coordinate of a source observed in WT mode if the Right Ascension and the Declination of the target are specified when processing the data. To take advantage of the estimated source average row coordinate for trap mapping purposes, in the latest round of calibration observations Tycho was observed in WT mode at three offsets pointings, at the average CCD row positions DETY=100, DETY=300 and

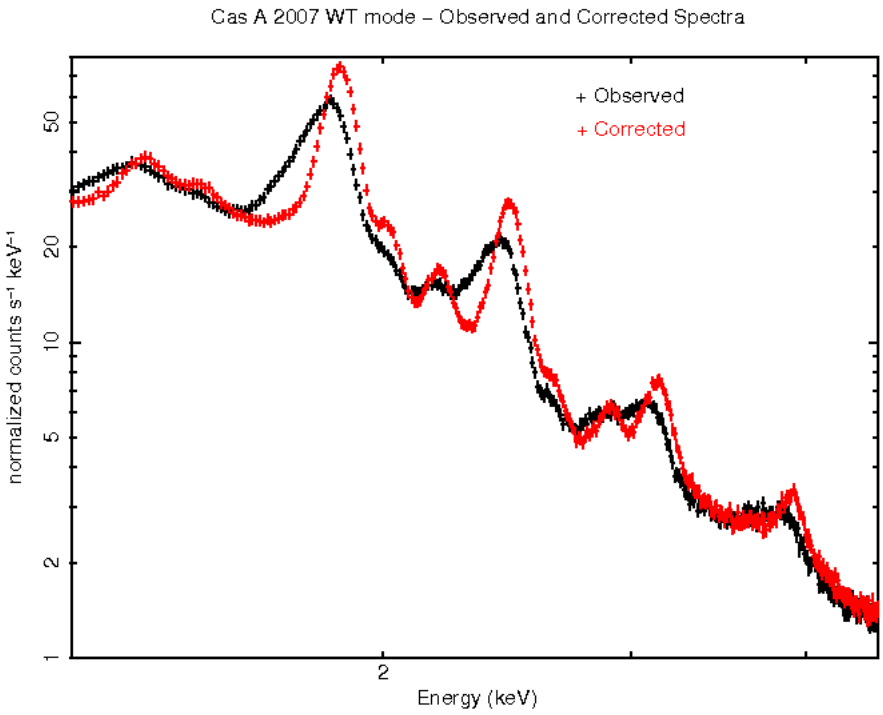

Figure C.7: Comparison of the observed and the trap corrected spectra extracted from WT observations of the Cas A SNR in October of 2007. The fit of the Silicon Kα line with an asymmetric Gaussian in IDL yielded a FWHM of 152 ± 13 eV for the observed spectrum and of 106 ± 3 eV for the corrected spectrum.

DETY=500, allowing the derivation of the energy offsets of three segments of each column (from DETY=[1,200], DETY=[201,400] and DETY=[401,600]). It is therefore recommended to specify the source's RA and Dec when running the *Swift-XRT* pipeline to obtain the best possible energy resolution in Windowed Timing mode.

Table 3 reports the FWHM values of the Si-Kα, S-Kα and Fe-Kα lines of the observed and the corrected WT spectra at different epochs, fitted in IDL with an asymmetric Gaussian. Figure C.7 compares the observed and corrected WT spectra of Cas A taken in October of 2007.

C.3 Trap offsets Energy dependence

The traps energy offset is a function of the incident photon energy. The energy dependence is modelled in the gain files with a broken power law (equation A.18). The Sulphur and Iron lines in Cas A and Tycho are used to derive the energy dependence above the break, while observations of the SNR E0102 with emission lines between 0.5 and 1 keV were used below the break.

The observed and trap-corrected spectrum of the SNR E0102 used for this analysis is shown in Figure C.8. PC mode observations yielded $\alpha 1 = 0.80$ and $\alpha 2 = 0.80$ before 2011 and $\alpha 1 = 0.80$ and $\alpha 2 = 0.85$ since 2011, with the break set at the reference energy of 1.856 keV; for WT mode observations before 2011, the measured slopes are $\alpha 1 = 0.70$ and $\alpha 2 = 0.50$, since 2011 the slopes are $\alpha 1 = 0.80$ and $\alpha 2 = 0.50$, with the break set to 3.0 keV.

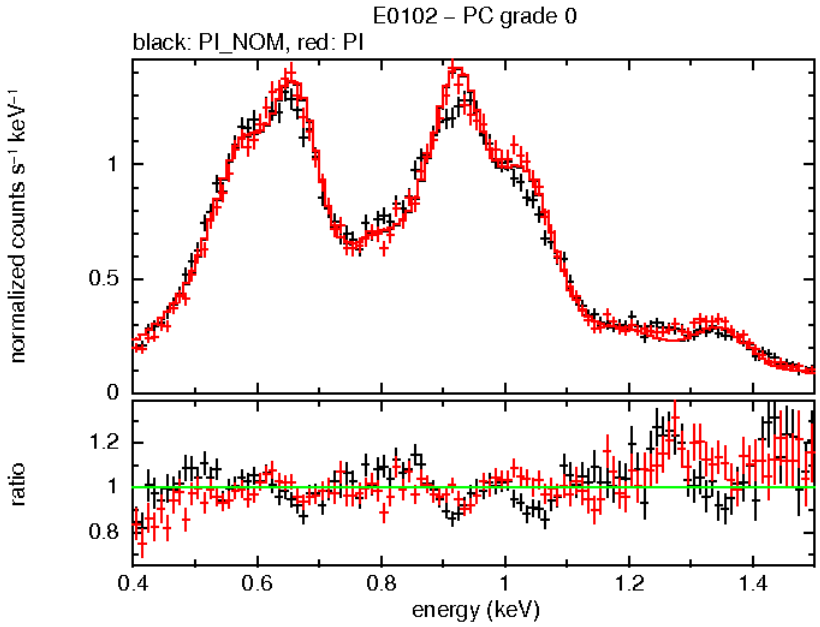

Figure C.8: Observed (black) and trap-corrected (red) spectrum of E0102 used to determine the CTE energy dependence at low energies. Dataset from 2008 to 2010 were merged to extract the spectra, and grade 0 events were selected. There is a definite improvement of the lines around 0.675, 0.915 and 1.035 keV in the trap corrected spectrum.

C.4 Trap corrections temperature dependence

The trap depths are temperature dependent because at higher CCD operating temperatures the dark current fills the traps. This behaviour can be seen, for example, from the corner sources analysis, where the high statistics allow the measurements of depth of individual traps at different temperatures, and can be observed in the long trap mapping Tycho observations in PC mode (Figure 5). In WT mode observations the effect is not seen because of the continuous and faster charge readout mode.

To model the observed temperature dependence we utilized the instrumental Nickel Kα line at 7.47 keV, by analysing every PC mode observation with an exposure time greater than 100 seconds. The data were processed merging all the observations taken during a year, removing point sources and extracting spectra selecting operating CCD temperatures with bins of 1 degree and by fitting the measured Nickel line energy. The results of this procedure can be seen for example for observations taken during 2014-2015 (Figure C.9, left panel vs right panel).

The energy shifts from the expected Nickel line energy were measured and are included in the gain files as GC3_TRAP coefficients at the reference temperatures of -75C, -61.5C and -48C for all epochs. The XRTCALPI software task applies a linear interpolation of the GC3_TRAP coefficients to derive the energy offset correction at all CCD temperatures. For all epochs, a non linearity of the temperature dependence is seen for CCD temperatures above -55C in the Nickel line analysis and the best modelling and correction of the temperature dependence was obtained by including distinct offsets trap tables at the reference temperatures of -75C, -61.5C and -48C in the gain files. The results of the applied corrections for the 2014-2015 dataset can be seen in the right panels of Figure C.9.

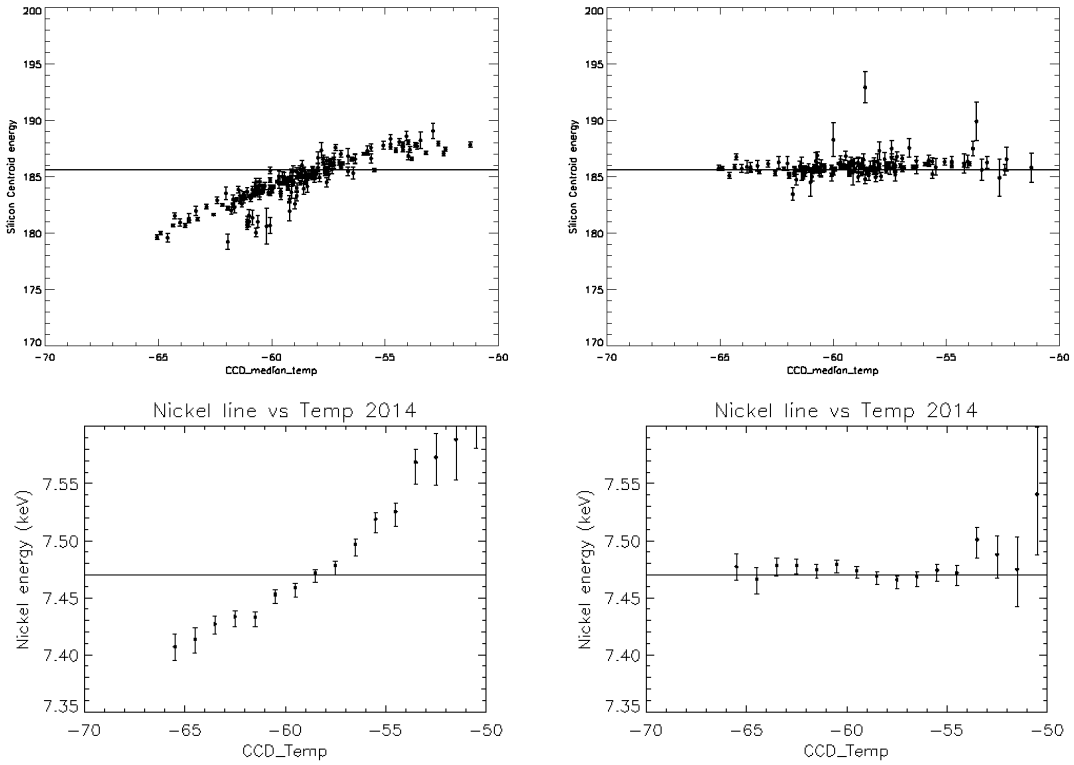

Figure C.9: The Tycho Silicon line (top left panel) and the instrumental Nickel line (bottom left panel), in the data rom the 2014-2015 campaign, show evidence of energy shifts from the expected values as a function of temperature. Processing the PC data with the updatd gain file, that includes temperature dependent trap tables, the Gaussian fits in both cases give energies close to the expected values at all temperatures, as can be seen in the right panels.

D References

Godet, O., Beardmore, A. P., Abbey, A. F., et al. 2007, SPIE, 6686
Godet, O., Beardmore, A. P., Abbey, A. F., et al. 2009, A&A, 494, 775
Pagani, C., Beardmore, A. P., Abbey, A. F., et al. 2011, A&A, 534, A20
Beardmore, A. P., et al. 2013, SWIFT-XRT-CALDB-09_v18
Beardmore, A. P., et al. 2014, SWIFT-XRT-CALDB-09_v19

E Previous Gain File Releases

Table E.1 lists the gain files made available through previous releases of the *Swift*-XRT CALDB. A web page summarising the releases, along with an archive of older release notes, is available from the University of Leicester's UKSSDC *Gain and RMF release summary* page.

Table E.1: Previous gain file releases.

FILENAME	VALID DATE	RELEASE DATE	REVISION
swxpcgain20010101v003.fits	01-Jan-2001	15-Oct-2004	003
swxpdgain20010101v003.fits	01-Jan-2001	15-Oct-2004	003
swxwtgain20010101v003.fits	01-Jan-2001	15-Oct-2004	003
swxpcgain20010101v004.fits	01-Jan-2001	10-Jan-2005	004
swxpdgain20010101v004.fits	01-Jan-2001	10-Jan-2005	004
swxwtgain20010101v004.fits	01-Jan-2001	10-Jan-2005	004
swxpcgain20010101v005.fits	01-Jan-2001	12-Oct-2005	005
swxpdgain20010101v005.fits	01-Jan-2001	12-Oct-2005	005
swxwtgain20010101v005.fits	01-Jan-2001	12-Oct-2005	005
swxpcgain20010101v006.fits	01-Jan-2001	1-Dec-2005	006
swxpdgain20010101v006.fits	01-Jan-2001	1-Dec-2005	006
swxwtgain20010101v006.fits	01-Jan-2001	1-Dec-2005	006
swxpcgains0_20010101v007.fits	01-Jan-2001	30-Jul-2007	007
swxpcgains6_20010101v007.fits	01-Jan-2001	30-Jul-2007	007
swxpdgains0_20010101v007.fits	01-Jan-2001	30-Jul-2007	007
swxwtgains0_20010101v007.fits	01-Jan-2001	30-Jul-2007	007
swxwtgains6_20010101v007.fits	01-Jan-2001	30-Jul-2007	007
swxwtgains0_20010101v008.fits	01-Jan-2001	21-Apr-2008	008
swxwtgains6_20010101v008.fits	01-Jan-2001	21-Apr-2008	008
swxpcgains0_20010101v008.fits	01-Jan-2001	07-Apr-2009	009
swxwtgains0_20010101v009.fits	01-Jan-2001	07-Apr-2009	009
swxpdgains0_20010101v008.fits	01-Jan-2001	07-Apr-2009	009
swxpcgains6_20010101v008.fits	01-Jan-2001	07-Apr-2009	009
swxwtgains6_20010101v009.fits	01-Jan-2001	07-Apr-2009	009
swxpcgains6_20010101v009.fits	01-Jan-2001	01-Dec-2009	009
swxwtgains6_20010101v010.fits	01-Jan-2001	01-Dec-2009	009
swxpcgains6_20010101v010.fits	01-Jan-2001	07-Jun-2011	010
swxwtgains6_20010101v011.fits	01-Jan-2001	07-Jun-2011	010
swxpcgains0_20010101v009.fits	01-Jan-2001	07-Jun-2011	010
swxwtgains0_20010101v010.fits	01-Jan-2001	07-Jun-2011	010
swxpdgains0_20010101v009.fits	01-Jan-2001	07-Jun-2011	010
swxpcgains6_20010101v011.fits	01-Jan-2001	09-Feb-2012	011
swxwtgains6_20010101v012.fits	01-Jan-2001	09-Feb-2012	011
swxpcgains0_20010101v010.fits	01-Jan-2001	09-Feb-2012	011
swxwtgains0_20010101v011.fits	01-Jan-2001	09-Feb-2012	011
swxpdgains0_20010101v010.fits	01-Jan-2001	09-Feb-2012	011
swxpcgains6_20010101v012.fits	01-Jan-2001	09-Feb-2013	012
swxwtgains6_20010101v013.fits	01-Jan-2001	09-Feb-2013	012
swxpcgains0_20010101v011.fits	01-Jan-2001	09-Feb-2013	012
swxwtgains0_20010101v012.fits	01-Jan-2001	09-Feb-2013	012
swxpcgains6_20010101v013.fits	01-Jan-2001	20-Dec-2013	013
swxwtgains6_20010101v014.fits	01-Jan-2001	20-Dec-2013	013
swxwtgains6_20010101v015.fits	01-Jan-2001	30-Jul-2014	014
swxpcgains6_20010101v014.fits	01-Jan-2001	03-Aug-2015	015
swxwtgains6_20010101v016.fits	01-Jan-2001	03-Aug-2015	015
swxpcgains6_20010101v015.fits	01-Jan-2001	10-May-2016	016
swxwtgains6_20010101v017.fits	01-Jan-2001	10-May-2016	016
swxpcgains6_20010101v016.fits	01-Jan-2001	01-May-2017	017
swxwtgains6_20010101v018.fits	01-Jan-2001	01-May-2017	017